Environmental Fluid Mechanics (2024) 24:465–488
https://doi.org/10.1007/s10652-024-10001-5

ORIGINAL ARTICLE

Self aeration and energy dissipation on a steep stepped chute: how does physical modelling compare to prototype observations?

Hubert Chanson[1] · **Jiayue Hu**[1]

Received: 15 October 2023 / Accepted: 17 July 2024 / Published online: 1 August 2024

Abstract

For the last five decades, a number of overflow stepped chutes were built because the staircase shape is conducive to reduced construction costs and increased rate of energy dissipation. The stepped chute operations are characterised by air-water flows that are highly turbulent flows with a large rate of energy dissipation, in comparison to smooth chutes. Herein, physical measurements were performed in a large-size 1 V: 0.80H stepped chute model, with a steep slope typical of modern concrete gravity dams. The results are compared to visual observations of prototype spillway operation under Froude similar conditions. The detailed two-phase flow measurements were conducted to characterise finely the self-aeration and air diffusion process downstream of the inception region of free-surface aeration. The bubble count rate profiles scaled with the instantaneous void fraction variance, and the relationship was biased close to the stepped invert under the influence of large-scale vortical structures. The rate of energy dissipation was carefully estimated based upon the two-phase flow measurements and the results are compared to earlier results on similar steep invert slopes and prototype data estimates. At the downstream end of the stepped chute, the rate of energy dissipation ranged from 43 to 46%, i.e. more than twice that on a smooth-invert chute for a similar chute length and discharge range.

✉ Hubert Chanson
h.chanson@uq.edu.au

[1] School of Civil Engineering, The University of Queensland, Brisbane, QLD 4072, Australia

Graphical abstract

Characteristics of self-aerated stepped chute flows for dc/h = 1.3—(I) Prototype flow at Hinze Dam (Re = 4.0 × 107); (II) Air-water flow properties in the large-size laboratory model (1:15) stepped spillway (Re = 6.1 × 105)

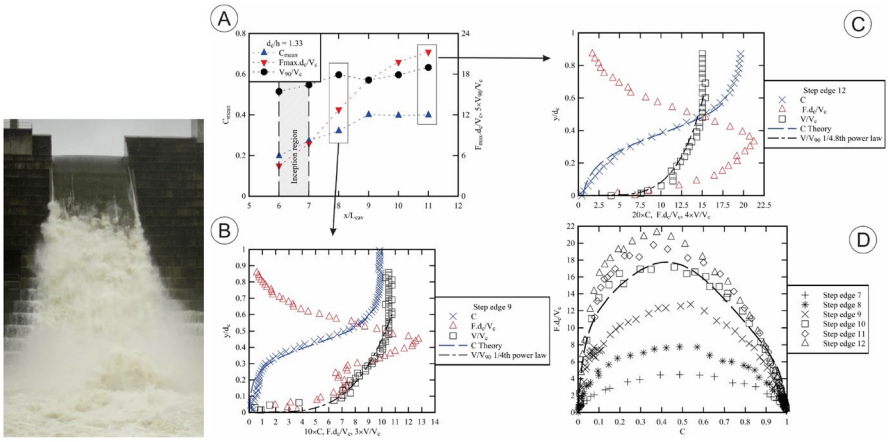

(I) (II)

Article Highlights

- **Air-water measurements were performed in a large-size 1V:0.8H stepped chute model.**
- **The results are compared to visual observations of prototype stepped chute operation under Froude similar conditions.**
- **The energy dissipation was estimated, taking into account the air-water flow properties inclusive of air-water pressure and velocity correction coefficients.**
- **The rate of energy dissipation ranged from 43 to 46%, i.e. more than double that on a smooth-invert chute.**
- **The contribution paves the way for future research to close the knowledge gap on self-aerated chute flows in full-scale structures.**

Keywords Self-aerated flows · Stepped spillways · Free-surface flows · Residual head · Physical modelling · Prototype observations

List of symbols

A	Clear-water flow area (m^2)
B	Rectangular channel width (m)
b	Characteristic value of the maximum range of the correction factor β
C	Time-averaged void fraction
C_{Fmax}	Local void fraction where $F = F_{max}$
C_{maen}	Depth-averaged void fraction: $C_{mean} = \frac{1}{Y_{90}} \times \int_{y=0}^{Y_{90}} C \times dy$

D_H Hydraulic diameter (m): $D_H = 4 \times A/P_w$
D_o Constant function of depth-averaged void fraction
D' Dimensionless turbulent diffusivity
d_c Critical flow depth (m)
d_I Flow depth (m) in the inception region
F Bubble count rate (Hz)
F_{max} Maximum bubble count rate (Hz)
g Gravity acceleration (m/s^2)
H Total head (m)
H_{max} Upstream total head (m)
H_{res} Residual head (m): $H_{res} = \Lambda \times d \times \cos\theta + z_o + \alpha \times \frac{V_{mean}^2}{2 \times g}$
h Vertical step height (m), measured from step edge to step edge
K Integration constant
L_{cav} Step cavity length (m): $L_{cav} = (h^2 + l^2)^{1/2}$
L_I Longitudinal location (m) of inception region
l Horizontal step length (m)
N Invert of velocity power law exponent
P_w Wetted perimeter (m)
Q Water discharge (m^3/s)
q Water discharge per unit width (m^2/s): $q = Q/B$
Re Reynolds number defined in terms of the mean velocity and hydraulic diameter: $Re = \rho \times \frac{V_{mean} \times D_H}{\mu}$
V Velocity (m/s)
V_c Critical flow velocity (m/s): $V_c = (g \times d_c)^{1/2}$
V_{mean} Cross-sectional mean velocity (m/s): $V_{mean} = Q/A$
V_{90} Characteristic air–water velocity (m/s) where $C = 0.90$
x Longitudinal distance (m) positive downstream
Y_{90} Characteristic air–water elevation (m) where $C = 0.90$
y Normal distance (m) measured perpendicular to and above the invert or pseudo-invert formed by the step edges
y' Dimensionless distance measured perpendicular to and above the invert or pseudo-invert formed by the step edges: $y' = y/Y_{90}$
α Air–water kinetic energy correction factor introduced in the energy equation: $\alpha = \frac{\int_0^{Y_{90}} (1-C) \times V \times \frac{V^2}{2} \times dy}{\frac{1}{2} \times V_{mean} \times d^3}$
ΔH Total head difference (m)
Λ Air–water pressure correction factor introduced in the energy equation: $\Lambda = \frac{\int_0^{Y_{90}} V \times \left(\int_y^{Y_{90}} (1-C) \times dy' + (1-C) \times y \right) \times dy}{V_{mean} \times d^2}$
λ_a Smallest discrete air element
λ_w Smallest discrete water element
μ Dynamic viscosity (Pa.s) of water
Ω Air–water pressure correction coefficient introduced in the energy equation: $\Lambda = \frac{\int_0^{Y_{90}} V \times \left(\int_y^{Y_{90}} (1-C) \times dy' + (1-C) \times y \right) \times dy}{V_{mean} \times d^2}$

θ Angle between longitudinal invert or pseudo-invert slope and horizontal
ρ Water density (kg/m^3)

Subscript
c Critical flow conditions
90 Characteristic air–water property where the void fraction is C = 0.90

1 Introduction

Dams must be equipped with a spillway system to discharge excess flood waters during major rainfall and runoff events [61, 77]. The spillway design must account for both a safe conveyance of flood flows and safe dissipation of the kinetic energy of the waters before the downstream end of the spillway structure, and before rejoining the downstream natural stream channel. During major flood flows, the rate of energy dissipation can be very large and exceeds the electrical outputs of large nuclear power plants [26]. As an illustration, a typical nuclear power reactor has an electrical output of 600 MW to 900 MW, although larger reactors can have electrical outputs of 1300 MW. At the Paradise Dam stepped spillway, the rate of energy dissipation was 2.8 GW on 20 December 2010, when the discharge was less than 10% of the PMF event. With the Hinze Dam stepped spillway during a 1:100 AEP flood event as on 31 March 2017 (+), the rate of energy dissipation corresponded to 108 MW. Both events were observed by Prof. Chanson.

With both dam spillways and urban storm waterways, the design of steep chutes may incorporate macro-roughness, such as a stepped invert, to reduce the size and cost of the downstream stilling structure [5, 16, 69]. Figure 1 presents some overflow stepped spillways which equip modern concrete gravity dams, and the figure caption lists the vertical step height h and chute slope. Stepped chutes have been in use for several millennia [20, 21]. During the 19th and up to the mid-twentieth centuries, a large amount of dam spillways were designed with a stepped chute worldwide. Stepped spillways have equipped gravity dams as well as embankment dams. During the last two centuries, embankment dam spillway designs encompassed overtopping embankment stepped spillways [23, 27, 41], stepped spillways on embankment dam abutment [20, 21], and unlined rock cascades [16, 21]. Examples of stepped spillways on embankment dam abutments include the Bilberry Dam spillway (UK, 1867), Malmsbury dam spillway (Australia, 1870), Gold Creek dam spillway (Australia 1890), Upper Coliban dam spillway (Australia 1903). All of which are still in use today, with Gold Creek dam being the world's first concrete stepped spillway [32]. Similarly, a number of gravity dams were equipped stepped spillway location with along embankment dam abutment directly excavated in the rock. For example, Tillot dam (France 1834), Pas-du-Riot dam (France 1873), Le Pont dam (France, 1882). Relevant reviews include Chanson (1995a, 2001), Novak et al. [61], Icold [49], and Hager et al. [44]

For the past 50 years, the advancements in concrete construction technology, including Roller Compacted Concrete (RCC) and Immersion Vibrated Roller Compacted Concrete (IVRCC), led to a strong interest for the stepped chute design, especially with concrete gravity dams. Figure 1 shows two RCC gravity dams equipped with an un-gated stepped chute. More, the combination of some re-evaluation of the Probable Maximum Flood (PMF) magnitude and local geographical constraints at a dam site can favour the stepped design because of the reduced footprint of the spillway structure for the same unit discharge, e.g. Hinze Dam, Australia.

Fig. 1 Concrete gravity dams equipped with stepped chute spillways (Photographs Hubert Chanson)—**A** Pedrogao Dam, Portugal on 4 September 2006, h = 0.6 m, 1 V:0.75H slope; **B** Riou Dam, France in June 1998, h = 0.43 m, 1 V:0.6H slope

During the last 20 years, a number of detailed laboratory studies were performed with stepped chute slopes ranging from 1 V:3.5H to 1 V:2H typical of embankment structures [31], Gonzalez [40], Bung [8], [48], Felder [38]. Physical studies on steeper stepped chutes covered slopes from 1 V:1H to 1 V:0.6H Chamani [13], Matos [58, 59], Boes [4], Zhang [91], [1, 2]. In the current study, new physical measurements were conducted in a large-size stepped spillway model, with a chute slope (1 V:0.80H) typical of modern concrete gravity structures. A key feature of the present physical measurements was the selection of boundary conditions and inflow conditions that were in similitude (geometry similarity, Froude similarity and Morton similarity) with spillway operation conditions during which field observations were conducted. Detailed two-phase flow measurements were conducted to finely characterise the self-aeration, the air–water flow properties and the rate of energy dissipation. The results are discussed in comparison to visual observations of large flood

flows over a 1 V:0.80H stepped spillway under Froude similar conditions, and other field observations of self-aerated flows.

2 Experimental approach, apparatus and instrumentation

2.1 Presentation

Any physical laboratory study aims to provide a reliable prediction of prototype hydraulic structure operation [45]. The modelling approach must be based upon the fundamental principles of similitude and dimensional analysis [3, 66, 78]. Considering the operation of a spillway chute (Fig. 2), a basic dimensional analysis shows a large number of relevant parameters [18, 84]. A true similarity would require having all dimensionless dependant parameters to be identical in model and prototype, and it is physically unachievable unless working at full-scale, i.e. field works.

Herein, the laboratory chute was designed as a simplified scale model of the Hinze Dam stepped chute [28, 62], in which field observations were conducted during the 2021 and 2022 floods. Figure 2 shows the Hinze Dam stepped chute during small events, thus providing a greater insight into the downstream stilling basin and its 3.2 m high baffle blocks, and Fig. 4 presents photographs of the Hinze Dam spillway during the 2021 and 2022 flood overflows. The physical facility had the same 1 V:0.80H chute slope (i.e. $\theta = 51.3°$) as the Hinze Dam stepped spillway, and the vertical step height h was scaled at 1/15th size of the prototype step dimensions. The physical model simplification was the crest, whereby the

Fig. 2 Hinze Dam stepped spillway, Australia during low overflows, h = 1.5 m, 1 V:0.80H slope—**A** q = 0.062 m^2/s, $d_c/h = 0.04$, $Re = 2.5 \times 10^5$, nappe flow regime on 25 April 2013 (Photograph Davide Wüthrich); **B** q = 1.7 m^2/s, $d_c/h = 0.45$, $Re = 6.8 \times 10^6$, transition flow regime on 3 May 2015 (Photograph Hubert Chanson)

prototype is equipped with an ogee crest starting with three 1 m high, whereas the physical model was instead equipped with a broad-crest with rounded edges followed by 14 identical steps.

The laboratory experiments were undertaken based upon a combined Froude and Morton similitude in a relatively large-size facility, operating at relatively large Reynolds numbers, defined in terms of hydraulic diameter, up to $Re = 7.8 \times 10^5$.

2.2 Experimental facility and instrumentation

The physical experiments were performed in a new stepped spillway physical model (1 V:0.80H) located at the University of Queensland (UQ). Three adjustable altering currents (AC) pumps delivered the flow into the 1.7 m deep and 5 m wide concrete basin. The water was smoothly converged by a 2.8 m long symmetrical sidewall profile before entering the 0.985 m wide test section surrounded by glass sidewalls. The concrete sidewall convergent with a contraction ratio of 5.08:1 resulted in a smooth and waveless flow into the upstream broad-crested weir (Chaokitka and [28, 29]). The weir was followed by a 1.4 m high stepped chute, with step height $h = 0.10$ m and step length $l = 0.08$ m. The steps were horizontal and made of smooth PVC.

The water discharge was estimated from the measured upstream head above crest based upon a careful discharge calibration (Chaokitka and [28, 29]). The upstream water level was recorded with a MeasumaX™ Single Column Digital Height gage with an accuracy of ± 0.05 mm. Clear-water flow depths were measured with a pointer gauge on the channel centreline. The air–water flow measurements were undertaken with a dual-tip phase-detection conductivity probe, designed and manufactured at the University of Queensland. The dual-tip probe was equipped with two identical needle sensors, each having an inner needle diameter of 0.25 mm and a longitudinal separation of probe tips of 9.0 mm in the streamwise direction. Each probe tip was sampled at 20 kHz for 45 s, with the sampling frequency and duration selection derived from previous sensitivity analysis results conducted at the University of Queensland (Felder [38], Zhang [91]). The distributions of air–water flow properties were recorded at different cross sections, with each vertical profile containing a minimum of 20 to 30 points on the chute centreline. The translation of the dual-tip phase-detection probe in the vertical direction was measured by a Mitutoyo™ digital scale unit with an accuracy of ± 0.025 mm.

The dual-tip phase-detection signal outputs were post-processed using a single threshold technique set at 50% of the voltage difference between air and water [11], Toombes [73], assigning an instantaneous void fraction value of 1 for air and of 0 for water. The time-averaged void fraction C was equal to the average time spent by the probe sensor in air relative to the total sampling time. The bubble count rate F was defined as the number of detected particles per unit time. The air–water interfacial velocity V was derived from a cross-correlation technique, based upon the time lag corresponding to the maximum cross-correlation coefficient between leading and trailing tip signals [10, 22, 67].

2.3 Experimental flow conditions

Prototype observations on the Hinze Dam stepped chute (Australia) took place during the March 2021 and February–March 2022 floods (Table 1 & Fig. 3). In 2021, a coastal trough developed near the North Coast of New South Wales. The trough deepened and expanded North along the South-East Queensland coast, with major rainfalls on 20–23

Table 1 Laboratory and prototype observations of self-aeration on steep (1 V:0.80H) stepped chutes

Reference	θ (°)	B (m)	h (m)	q (m^2/s)	d_c/h	Re	Geometry	Comments
Present study UQ22	51.3	0.985	0.10	0.009–0.195	0.2–1.58	2.8×10^4–7.8×10^5	Stepped PVC chute	Air–water flow feature observations
				0.0954	0.98	3.8×10^5		Dual-tip phase-detection probe (∅ = 0.25 mm) measurements
				0.1523	1.33	6.1×10^5		
				0.1959	1.58	7.8×10^5		
Hinze dam	51.3	12.25	1.5				Stepped concrete chute	Prototype observations
				5.86	1.01	2.3×10^7		27 March 2021
				9.05	1.35	4.0×10^7		23 March 2021 (heavy rainfall)
				9.05	1.35	4.0×10^7		4 March 2022
				11.4	1.58	5.1×10^7		24 March 2021
				11.65	1.60	5.2×10^7		3 March 2022
Zhou [95]	51.3	0.2	0.04	0.012–0.189	0.024–3.8	4.6×10^4–7.5×10^5	Stepped chute	Laboratory study
Wahrheit-lensing (1996)	51.3	0.5	0.04	0.01–0.09	0.5–2.3	4.0×10^4–3.6×10^5	Stepped chute	Laboratory study
Chamani and Rajaratnam [14]	51.3	0.3	0.125	0.08–0.20	0.7–1.3	3.2×10^5–8.2×10^5	Stepped chute	Laboratory study

B, chute width; d_c, critical flow depth; h, step height; q, unit water discharge; Re, Reynolds number defined in terms of hydraulic diameter; θ, angle between invert or pseudo-invert slope and horizontal; N/A, not available

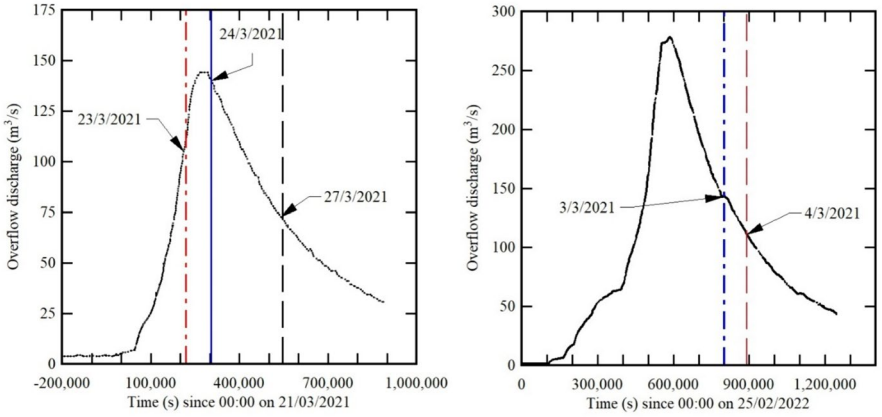

Fig. 3 Spillway discharge at Hinze Dam stepped spillway, Australia during the 2021 and 2022 flood events

March 2021. The daily total at a nearby coastal station exceeded 100 mm with a rainfall total of 546.8 mm. The 2022 floods in South-East Queensland were the result of an unusual weather system, which moved slowly south from the Sunshine Coast to the Gold Coast, before continuing into New South Wales. The Hinze dam catchment received over 433 mm of rain in 72 h between 24 and 27 February 2022. Both the 2021 and 2022 weather systems led to some large overflows at the Hinze Dam spillway (Fig. 3). Further details on the observation method were reported in Chanson (2022a,b).

In the simplified scale model of the Hinze Dam stepped chute, basic observations were conducted for unit discharges between 0.009 and 0.195 m^2/s (Table 1). Detailed air–water flow measurements were performed in the stepped chute model for three different water flow rates, corresponding to dimensionless discharges $d_c/h = 1.0$, 1.33 and 1.58, with d_c the critical flow depth $d_c = (q^2/g)^{1/3}$, q the unit discharge, g the gravity constant and h the vertical step height. These flow conditions were selected to be Froude-similar to the prototype spillway observations (Fig. 3, Table 1), with the same dimensionless discharges d_c/h, while the model Reynolds numbers were $Re = 3.8 \times 10^5$, 6.1×10^5 and 7.8×10^5 (Table 1). The three flow conditions corresponded to some skimming flow.

2.4 Basic observations and air–water flow features

At low flow rates corresponding to dimensionless discharges $d_c/h < 0.45$, the water flowed down the laboratory stepped chute as a series of free-nappes without hydraulic jump: i.e. a nappe flow regime. Figure 2A shows the prototype spillway operating for such a nappe flow regime. For $0.45 < d_c/h < 0.9$, the overflow discharge was highly turbulent, with very strong splash and intense spray, i.e. a transition flow. Figure 2B presents a photograph of transition flow in the prototype spillway; we can see the spray and splashing overtopping the training walls. For dimensionless discharges $d_c/h > 0.9$, the flow skimmed over the pseudo-bottom formed by the step edges and the streamlines were approximately parallel to the invert: i.e., a skimming flow (Fig. 4). A turbulent boundary layer formed downstream of the spillway crest, and the free surface features varied longitudinally along the steep chute. Once the outer edge of the developing boundary layer reached the free surface region, the turbulent shear stresses operating close to the free surface dominated over the

Fig. 4 Comparative photographs of prototype and laboratory model stepped chute (1 V:0.80H) flows: Hinze Dam stepped spillway (Left) and UQ stepped chute model (Centre & Right) (Photographs Hubert Chanson)—On the prototype photographs, the mean location of free-surface aeration onset was superposed in yellow—All photographs are high-shutter speed (i.e. less than 1 ms exposure time), **A** $d_c/h = 1$, $Re = 2.3 \times 10^7$ (Hinze Dam) and $Re = 3.8 \times 10^5$ (UQ model), **B** $d_c/h = 1.35$, $Re = 4.0 \times 10^7$ (Hinze Dam) and $d_c/h = 1.33$, $Re = 6.1 \times 10^5$ (UQ model), **C** $d_c/h = 1.6$, $Re = 5.1 \times 10^7$ (Hinze Dam) and $Re = 7.8 \times 10^5$ (UQ model)—Centre: top view of laboratory chute flow (arrow show flow direction)

combined effects of surface tension and buoyancy, leading to air entrainment [37, 89]. A close inspection of the cavity vortices, in the laboratory model, highlighted irregular ejections of fluid from the cavity into the mainstream towards the upper portion of the vertical step face, as well as the replacement of cavity fluid along the step edge, indicating a high degree of mainstream-cavity interaction, as noted by Rajaratnam [64] and Chanson et al. [33]. The flow was self-aerated downstream of the region where free-surface aeration began, and the air–water flow measurements revealed that the velocity profiles were fully-developed.

Visually, the laboratory flow conditions were similar to prototype observations on 1 V:0.80H stepped chute, as illustrated in Fig. 4. In Fig. 4, the geometric scaling ratio between prototype and laboratory model is 15:1, and the chute aspect ratio B/h is similar: i.e., B/h = 8.2 and 9.85 in the prototype and model respectively with B the chute breadth. For three different dimensionless discharges d_c/h, the photographs present a side-by-side comparison of prototype and laboratory stepped chute flows with the same chute slope (Fig. 4). The main visual differences between laboratory and full-scale observations were (a) the dark brown colour of the prototype flow at the upstream end, and (b) the intense air–water turbulence in the self-aerated flow region of the prototype spillway chute. The former indicated some sediment-laden inflow into the spillway structure and is common in prototype hydraulic structures. The latter might hint for a more dynamic and energetic air entrapment process in the prototype, implying that the air bubble diffusion process in laboratory might not be in similitude with that in large prototype spillways. This aspect was previously highlighted and argued by Chanson (1995b, 1997) and Zhang and Chanson [93].

2.5 Inception of free-surface aeration

On a steep chute, the onset of free-surface aeration takes place when the outer edge of the developing boundary layer starts to interact with the free-surface [60, 83]. The interactions are very dynamic transient processes in prototype chutes [25, 28], and free-surface aeration is caused by the very strong turbulence acting next to the free surface in the water phase [7, 24, 37]. Several studies emphasised the role of longitudinal vortices developing during the rapid flow acceleration at the spillway crest and from the first step edge, leading to the instantaneous deformation of the free surface as a result of vortical structure interactions further downstream [56, 76], Zabatela and Bombardelli 2020).

The location of the inception region of free-surface aeration was clearly seen in both prototype and model stepped chutes, as illustrated in Figs. 2 and 4. At the Hinze Dam, the prototype data were based upon photographic and cinematographic observations recorded during the flood events and compared to well-defined ground reference points [28]. Both the location of the inception region and water depth at inception were estimated as the mean value obtained from dozens of high-resolution photographs and several video movies. Some differences of results were seen for the prototype data corresponding to $d_c/h = 1.6$

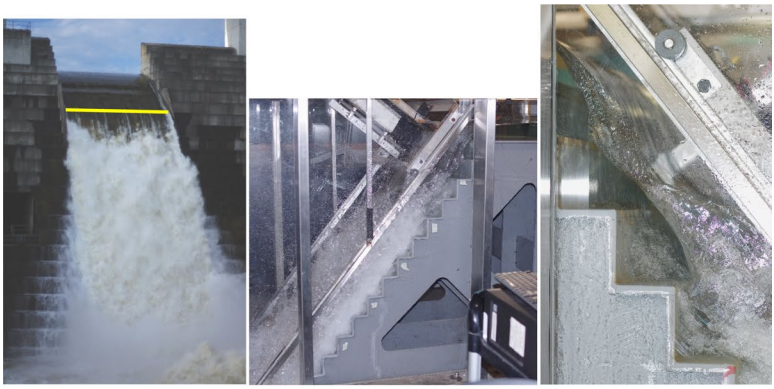

(A) $d_c/h = 1$, $Re = 2.3\times10^7$ (Hinze Dam) and $Re = 3.8\times10^5$ (UQ model)

(B) $d_c/h = 1.35$, $Re = 4.0\times10^7$ (Hinze Dam) and $d_c/h = 1.33$, $Re = 6.1\times10^5$ (UQ model)

(C) $d_c/h = 1.6$, $Re = 5.1\times10^7$ (Hinze Dam) and $Re = 7.8\times10^5$ (UQ model) - Centre: top view of laboratory chute flow (arrow show flow direction)

(3 March 2022) and $d_c/h = 1.58$ (24 March 2021). In both cases, the discharge estimates were accurate, but the weather conditions were markedly different, with heavy rainfall and rainstorms on 3 March 2022 in contrast to sunny weather on 24 March 2021. It is conceivable that the weather conditions adversely impacted onto the quality of the photographs and video movies, and on the quality of the data interpretation on 3 March 2022.

Both laboratory and prototype data sets are reported in Fig. 5A, showing a close agreement. They are further compared to previous data sets with the same chute slope (Table 1), highlighting an increasing distance of the inception region with increasing flow rate. The finding was close to the relevant literature (e.g. [14], Chanson et al. [26]). The dimensionless inception depth data d_I/h in the inception region are presented in Fig. 5B. The

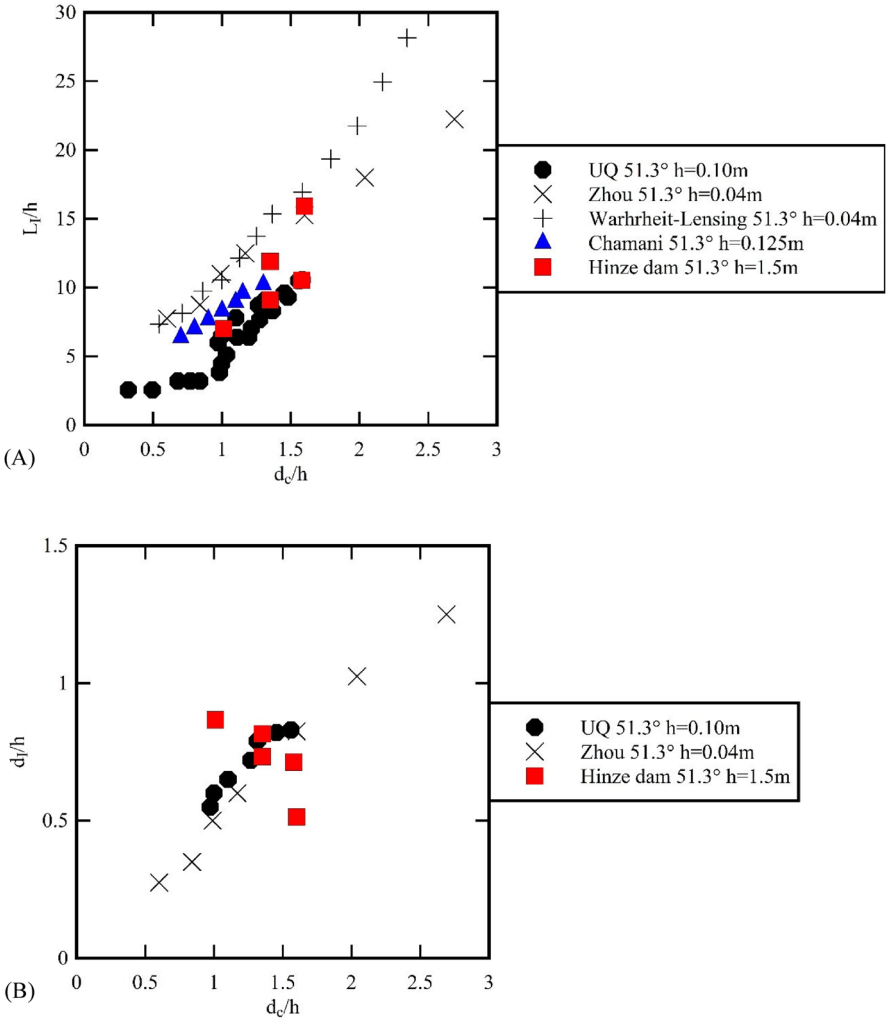

Fig. 5 Location and water depth at the inception region of free-surface aeration on 1 V:0.80H steep stepped chutes—Comparison between prototype data and laboratory model data (Table 1)

difference between prototype and laboratory model data is puzzling, but "*nature is the final jury*" [65]. Importantly, it is critical to stress the excellent accuracy of the Hinze Dam data set linked to the access ease [28], as well as some difference in stepped chute shape between the ogee profile at Hinze Dam and the simplified laboratory model. Noteworthy, the trend of an increasing trend of d_I/h with d_c/h is primarily based upon laboratory data. Except for the Hinze Dam, the few prototype data in terms of d_I/hare very scattered (Chanson et al. [26], p. 52).

2.6 Air–water flow properties

The air–water flow property measurements were conducted at all step edges downstream of the inception region of free surface aeration. In the direction normal to the flow, measurements were obtained above the pseudo-bottom formed by the step edges up to the upper spray area. Typical results are presented in Fig. 6, where d_c is the critical flow depth, V_c is the critical velocity, C_{mean} is the depth-averaged void fraction defined in terms of 90% void fraction, F_{max} is the maximum bubble count rate in the section, and V_{90} is the characteristic air–water velocity at 90% void fraction.

The void fraction profiles followed an inverted S-shape, illustrated in Fig. 6B and C. In Fig. 6B and C, the void fraction data are compared to the advective diffusion theoretical model of Chanson and Toombes [31]:

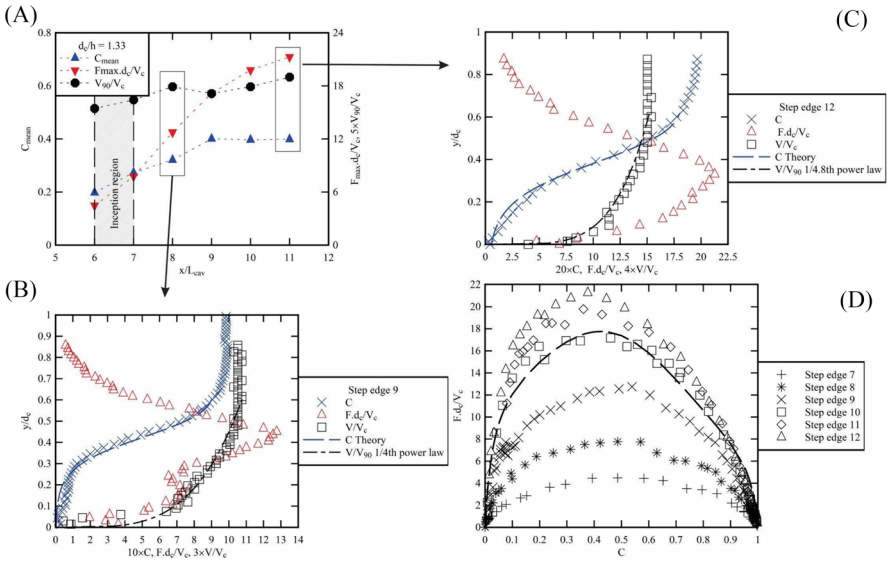

Fig. 6 Air–water flow properties in the large-size laboratory model stepped spillway (1 V:0.80H) for $d_c/h = 1.33$ and $Re = 6.1 \times 10^5$—**A** Longitudinal variation of depth-averaged void fraction C_{mean}, dimensionless maximum bubble count rate $F_{max} \times d_c/V_c$, and dimensionless characteristic air–water velocity V_{90}/V_c; **B** Dimensionless distributions of void fraction, bubble count rate and interfacial velocity at step edge 9; **C** Dimensionless distributions of void fraction, bubble count rate and interfacial velocity at step edge 12; **D** Dimensionless relationship between bubble count rate and void fraction at several step edges in the air–water flow region

$$C = 1 - \tanh^2\left(K - \frac{y'}{2 \times D_o} + \frac{\left(y' - 1/3\right)^3}{3 \times D_o}\right) \text{for } 0 < y' < 1 \quad (1)$$

where y' = y/Y_{90}, y is the distance normal to the pseudo-invert formed by the step edges, Y_{90} is the distance when the void fraction is 90%, and the dimensionless turbulent diffusivity D' profile is assumed to be:

$$D' = \frac{D_o}{1 - 2 \times \left(y' - 1/3\right)^2} \quad (2)$$

with D_o a function of the depth-averaged void fraction and K an integration constant:

$$C_{mean} = 0.7622 \times \left(1.0434 - e^{-3.614 \times D_o}\right) \quad (3)$$

$$K = \tanh^{-1}\left(\sqrt{0.1}\right) + \frac{1}{2 \times D_o} - \frac{8}{81 \times D_o} \quad (4)$$

The void fraction data implied the strong flow aeration and fragmentation of the skimming flow regime, with increasing aeration with increasing distance downstream of the inception region of free-surface aeration. This is seen in Fig. 6A with the longitudinal variation in depth-averaged void fraction C_{mean}, reaching about 40% near the downstream end of the chute, for all three discharges (Table 1).

The air–water flow fragmentation may be quantified by the bubble count rate, also called bubble frequency and bubble impaction rate [67]. At each step edge, the distributions of bubble count rate presented a marked maximum, seen in Figs. 6B and C. The bubble count rate profiles scaled with the instantaneous void fraction variance, reaching a maximum for void fraction between 0.35 and 0.5 (Fig. 6). The relationship between bubble count rate and void fraction presented a pseudo-parabolic shape, although it was biased close to the invert under the influence of large-scale coherent structures (Fig. 6D). The present data followed closely a theoretical model [75]:

$$\frac{F}{F_{\max}} = \frac{1}{\alpha \times \beta} \times \frac{C \times (1 - C)}{C_{F\max}^2} \quad (5)$$

with C_{Fmax} the local void fraction where the bubble count rate is maximum ($F = F_{max}$), and α' and β' two correction factors that are functions of the local void fraction such as:

$$\alpha' = 1 + \left(\frac{\lambda_w}{\lambda_a} - 1\right) \times C \quad (6)$$

$$\beta' = 1 - b \times (1 - 2 \times C)^4 \quad (7)$$

with the ratio λ_w/λ_a being a constant linked to the ratio of the smallest discrete air element to smallest discrete water element in the mixture, and b a characteristic value of the maximum range of the correction factor β': i.e., 1-b < β' < 1. Note that α ' and β ' are related to the local void fraction C_{FMax}:

$$\alpha' \times \beta' = \frac{1 - C_{F\max}}{C_{F\max}} \tag{8}$$

Equation (5) is shown in Fig. 6D for step edge 10. All the present data showed an increasing maximum bubble count rate with increasing downstream distance, without reaching an asymptotic value (Figs. 6A and D). The finding implied that the air–water structure typology, and the bubble-turbulence interactions, continued to evolve and did not reach an equilibrium. This longitudinal pattern with monotonic increase in bubble count rate was observed in earlier studies (e.g. [88], Bung [8]) and might be linked to scaling issues [24, 39].

The air–water velocity profiles showed a power law for void fractions less than 90%:

$$\frac{V}{V_{90}} = y'^{1/N} 0 < y' < 1 \tag{9}$$

as illustrated in Fig. 6 B and C. The power law exponent 1/N varied between 1/3.5 and 1/6, in line with experimental observations in steep stepped spillway models by Matos [58, 59] [1 V:0.75H] and Boes [20] [1 V:0.84H]. In contrast, observations on embankment dam stepped spillway models yielded a velocity power law exponent 1/N between 1/7 and 1/12 (Gonzalez [40], Bung [8], Felder [38]). The difference in velocity profile shape was very likely linked to differences in momentum transfer between the main flow and the cavity region, associated with differences in step cavity shapes and different step cavity recirculation processes, between steep concrete gravity dam and embankment dam stepped spillways.

2.7 Energy dissipation and residual head

In a skimming flow down a steep stepped chute, the dissipation of the kinetic energy is primarily a form drag process driven by the cavity recirculation in the stepped cavities [33, 64]. Both the fluid acceleration and the boundary layer development in the non-aerated region affect the rate of energy dissipation and residual energy. In the present study, the rate of energy dissipation was estimated, taking into account the air–water flow properties inclusive of the air–water pressure and velocity correction coefficients [1]. That is, the residual head was estimated as:

$$H_{res} = \Lambda \times d \times \cos\theta + z_o + \alpha \times \frac{V_{mean}^2}{2 \times g} \tag{10}$$

with d the equivalent clear-water depth, z_o the bed elevation, and α and Λ some air–water kinetic energy and pressure correction coefficients respectively [34]. The present results are reported in Figs. 7 and 8.

At the downstream end of the stepped chute, the rate of energy dissipation $\Delta H/H_{max}$ ranged from 0.43 to 0.46 (Fig. 7). In comparison, for a similar chute slope, chute length and unit discharge range, the smooth-invert chute flow would be non-aerated [42, 85], and experimental data [42] and theoretical calculations [19] yield a rate of energy dissipation between 0.1 and 0.2, consistent with steep smooth invert prototype tests [6].

The present data are further reported in Fig. 8 in terms of the dimensionless residual head H_{res}/d_c as a function of the dimensionless longitudinal distance. The physical data are

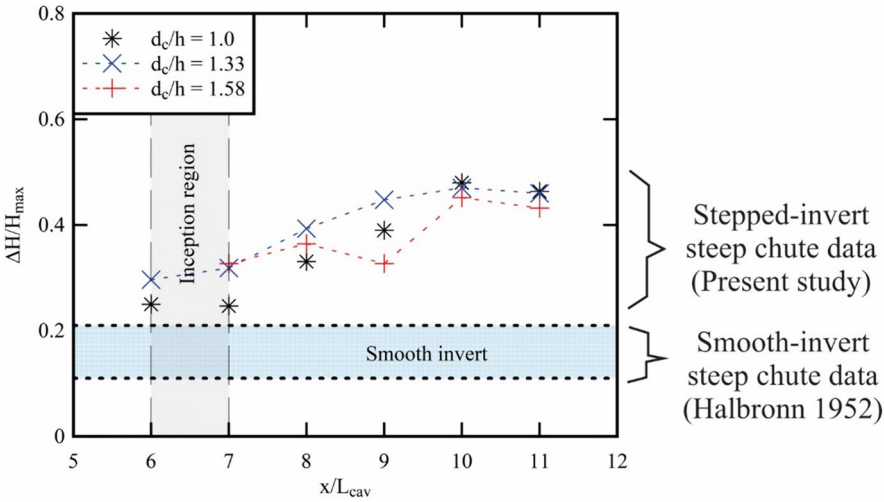

Fig. 7 Energy dissipation in the large-size laboratory model stepped spillway (1 V:0.80H) taking into account the air entrainment: longitudinal variation of dimensionless rate of energy dissipation H/H_{max} and comparison with steep smooth chute data [42]

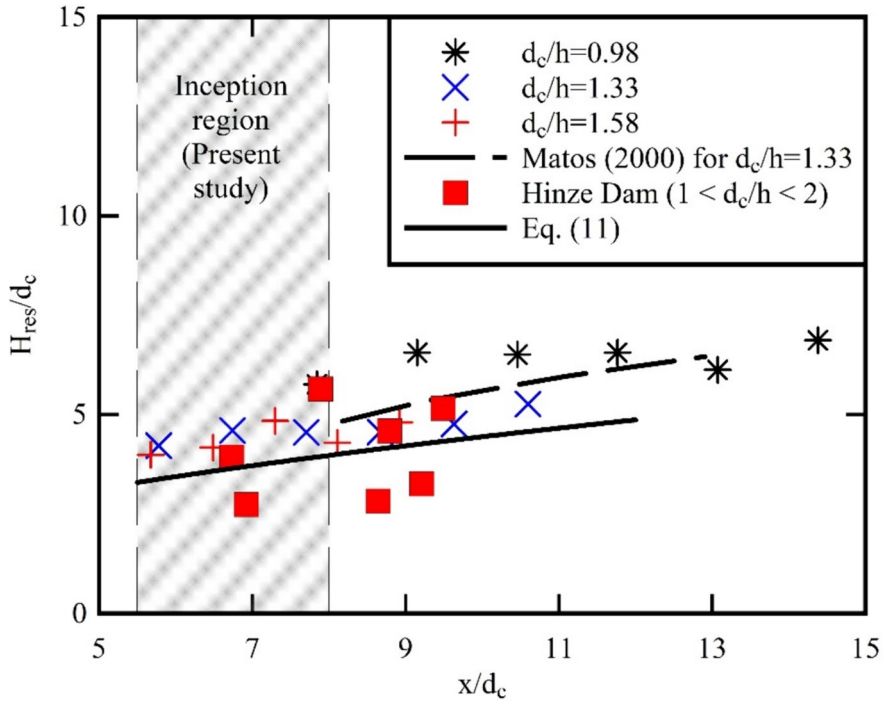

Fig. 8 Longitudinal variation of dimensionless residual energy H_{res}/d_c in the large-size laboratory model stepped spillway (1 V:0.80H) taking into account the air entrainment and at the Hinze Dam spillway—Comparison with the design method of Matos (2000) for steep stepped chutes and with Eq. (11)

compared to Hinze Dam spillway data estimated in the inception region for $1 < d_c/h < 2$, which were best correlated by:

$$\frac{H_{res}}{d_c} = 1.406 \times \sqrt{\frac{x}{d_c}} \text{for } 1 < d_c/h < 2 \quad (11)$$

with Eq. (11) drawn in Fig. 8. The Hinze Dam prototype data compared reasonably well to both the air–water flow data in laboratory and the design method of Matos [59] for steep concrete gravity dam stepped spillways. Despite some difference between prototype and laboratory data, both data sets presented a similar trend and the agreement is notable. The results may be used to estimate the residual head for a given step height, chute height and design unit flow.

Altogether, the present data showed an increasing residual head with increasing discharge (Fig. 8 and Eq. (11)), linked to the further downstream location of the inception region at larger discharges. For much larger discharges, the stepped chute free-surface flow would become non-aerated, and the flow would not be fully-developed before the downstream end of the spillway. The residual head would be significantly larger and a different design calculation method would be required, e.g. Chanson [21], Gonzalez [40].

3 Discussion

Today, there remains a critical need for more prototype spillway data sets, as discussed more than 40 years ago (Kobus [52], [36, 54]). This knowledge gap has been very rarely addressed, except for too few seminal studies, e.g. at Aviemore Dam, Grande Dixence Dam [10, 79]. The present study aimed to add to the topic with a direct comparison between laboratory and prototype data, with the physical measurements being conducted using boundary conditions and inflow conditions that were in similitude with prototype spillway operation conditions of a large dam during which field observations were conducted. To date, one may wonder about the apparent lack of progress to address the knowledge gap in the last four decades.

For the past two decades, alone, there have been numerous hydraulic structure failures [63, 80] and a key challenge is the absence of prototype high-speed flow data sets during major flood events and the re-iterated need for "*new field measurements, performed* in situ *at the full-scale"* because "*no prototype data means no definite validation of any kind of modelling!*" [25], p. 237). In high-velocity free-surface chute flows, some large amount of air may be entrained and advected with the water, forming a complicated two-phase mixture (Figs. 2 and 4). The resulting self-aerated flows make an intricate air–water mix with air entities within water, water droplets surrounded by air, and more complicated air–water structures for void fractions about 40–60% [7, 18]. For the last six decades, moderately successful analytical models of the void fraction distribution and air bubble diffusion in self-aerated flows have been formulated to describe the development of air entrainment and interfacial aeration in high-velocity free-surface flows. Noteworthy among these are the diffusion analyses of Straub and Anderson [70], Wood [82], Chanson (1995b, 1997), Chanson and Toombes [31] and Zhang and Chanson [93], and the free-surface theories of Killen [51], Toombes and Chanson (2007, 2008) and Kramer and Valero [55]. In parallel, a number of mechanistic air bubble entrainment models were implemented computationally and successfully tested in wave breaking [12, 46, 57]. The proliferation of so many theories

might suggest that there still is not unanimity on the question of precisely what processes are responsible for the inception and early development of self-aeration.

On the other hand, detailed high-speed and ultra-high-speed video imaging records successfully showed no discontinuity in the air–water flow structure from the bubbly flow region next to the invert up to upper free-surface where the void fraction reaches 90% to 95% [2, 9, 94]. The outcome was consistent with fine intrusive two-phase flow measurements of void fraction, bubble frequency and interfacial velocity (Matos [58], Boes [4], Zhang [91], Present study). In the case of air–water flows in steep prismatic chutes, the available physical data, with both prototype and laboratory data sets, are adequate to predict the principal features of air–water flows [15, 18, 83, 84], Matos [59], Gonzalez [40], Present study). The inception region is characterised by a brutal transition from non-aerated to self-aerated flow motion as evidenced in prototype spillways (Keller [50], [10, 28]. Further downstream of the inception region, and at a given location, the air bubble turbulent diffusion normal to the invert is counterbalanced by the buoyancy effect, and the longitudinal variation of mean air concentration is gradual. Both prototype and large-size laboratory data sets reported a smooth, continuous, prismatic increase in both void fraction and air–water interfacial velocity with increasing distance normal to the invert [10], Matos [58], [31]. Several experimental data sets showed a pseudo-parabolic relationship between local void fraction and bubble count rate across the entire air–water column [31], Gonzalez [40], [75], Bung [8], Present study). Such a quasi-parabolic relationship implied a pseudo linear relation between the root mean square of instantaneous void fraction and bubble count rate. By extension, the finding implied a monotonic relationship between bubble frequency and interfacial turbulence intensity [92].

A number of prototype observations emphasised that the prototype self-aerated flows are highly unsteady: at Aviemore Dam's smooth-invert spillway, Keller ([50], p. 122) highlighted "*the extremely broken, unsteady nature of the surface of an aerated flow*"; at the Hinze Dam's stepped spillway, "*visual, photographic, and cinematographic observations suggested that the instantaneous location of the inception region varied with both time and transversal location*" [28], p. 9). In parallel, a number of field studies showed that high-velocity air–water chute flows are three-dimensional: "*the unstable nature of the flow surface is evident from the vastly dissimilar surface aeration patterns, implying that the assumption of two-dimensional flow is not altogether justifiable near the surface*" (Keller [50], pp. 102–104); "*the effects of a multitude of irregular high-energy vortices result in a contorted three-dimensional free surface*" [53], p. 4),"*the OF surface velocity maps further suggested the presence of longitudinal "streets" of lower surface velocities, with streaks of faster flowing fluid in between, near the inception region*" [29], p. 5). The strong three-dimensionality of the air–water free-surface flows implies that the inflows into a downstream energy dissipator include some regions of kinetic energy peaks. The finding is directly relevant to the safe design of downstream energy dissipators (e.g. Figs 1, 2) and infers the need for some form of safety factor in the design process.

Intriguingly, the effects of chute sidewalls on the air–water flow characteristics were rarely investigated and documented. Notable exceptions included the laboratory works of Halbronn et al. [43] and Straub and Lamb [71] in smooth-invert chute flows, Zhang and Chanson [94] on stepped chute flows, Tang et al. [72] and Wüthrich et al. (2020, 2023) in hydraulic jumps, and Shi et al. [68] in transient breaking bores. In steady flows, all the air–water flow data showed systematically a lesser depth-averaged void fraction, a slower air–water interfacial velocity, and a lesser bubble count rate next to the sidewall boundaries, compared to the chute centreline data [43, 72, 86, 87, 94]. Very detailed transverse measurements implied the existence of some lateral air–water boundary layer for a

relatively wide range of air–water flow typology and air–water flow conditions [72, 86, 87]. The existence of these well-documented sidewall effects raises a number of questions about any assumption that sidewall data could be representative of the centreline data. This constitutes an important challenge for the applicability of optical techniques and associated image-processing techniques based on pictures and videos collected near the sidewalls, i.e. in laboratory.

4 Conclusion and future outcomes

The current study focused on the hydraulics of air–water flows on a steep stepped chute with a 1 V:0.80H slope, typical of concrete gravity structures. The goals were to accurately estimate the hydrodynamics, interfacial aeration, and energy dissipation of a steep stepped stream in a large-size facility, as well as to compare laboratory and prototype flow features under identical Morton- and Froude-similar conditions. In both prototype and laboratory, the upstream flow motion was a non-aerated skimming flow motion and the free-surface appeared relatively smooth up to the inception region of free-surface aeration. Downstream of the inception region, the free-surface became extremely turbulent and strong air entrainment was observed. The laboratory experiments were consistent with prototype observations for Froude-similar flow conditions and identical slope, although the air–water surface turbulence in the self-aerated flow region appeared to be more intense in the prototype spillway chute (Fig. 4).

Detailed air–water flow measurements were performed at the step edges downstream of the region when the free-surface aeration occurred. The laboratory data demonstrated consistent patterns in skimming flow regimes, despite quantitative variations. The void fraction distribution compared well with a theoretical model of advective diffusion. The relationship between void fraction and bubble count rate presented a quasi-parabolic shape, for void fractions between 0 and 100%, skewed towards the invert. The velocity profiles tended to follow a power law from the invert up to the location where the void fraction equal 90%, with an exponent typical of steep stepped spillways, which differed from observations on embankment dam stepped spillways. The rate of energy dissipation and residual energy data are presented for fully-developed air–water flows on steep stepped spillways, showing a massive increase in rate of energy dissipation along the steep chute compared to smooth-invert chute flows: i.e. two to four times more than that on a smooth-invert chute for a similar chute length and discharges.

A comparison between self-aerated flow prototype and laboratory chute observations, including the present study, emphasised some smooth distributions in terms of the air–water flow properties from the bubbly flow region next to the invert up to the upper free-surface where the void fraction reaches 90% and more, without any form of discontinuity. Prototype observations showed the occurrence of highly unsteady transient processes, and the air–water flows presented some three-dimensional velocity field, with direct implication in terms of safe design of downstream stilling structures. Sidewall effects were recently evidenced in terms of air–water flow properties, including void fraction, bubble count rate and air–water velocity, challenging the applicability of sidewall-based optical techniques image-processing techniques. In this context, the current contribution paves the way for future research to close the knowledge gap on self-aerated chute flows in full-scale structures. Further advancements would require newer prototype studies and field observations during major floods. Field measurements should encompass traditional approaches,

e.g. intrusive probe data, as well as newer non-intrusive methods, e.g. optical techniques. In itself, the range of potential field work measurement equipment is very broad, and could lead to a longer argumentation. Potential field measurement sensors in dam spillways may include pressure sensors located on steps, pressure impact probe and ADCP in developing flow region, phase-detection probes in air–water flow region, as well as ultrasonic displacement meters, video imaging (e.g. LSPIV, Optical flow (OF), RGB-D sensor), laser techniques (e.g. LiDAR), Lagrangian sensors (e.g. robot fish with bionic or chemical sensors).

The present research is a step forward in the design of steep stepped spillways, particularly regarding self-aerated flow characteristics Since the experimental data were collected in large-size hydraulic model and successfully compared to prototype data, some robust expressions for the characteristics of self-aeration inception region and rate of energy dissipation on steep stepped spillways are now available.

Acknowledgements The authors acknowledge the technical assistance of Jason Van Der Gevel and Stewart Matthews, The University of Queensland. HC thanks Dr Davide Wüthrich, TU Delft, for providing Fig 2A. The authors acknowledge the helpful comments of the anonymous reviewers.

Author contributions HC conducted the project supervision, project's scope development, the field observations and data re-analysis. He prepared the first draft of the manuscript. JH collected and processed the data set UQ22. She provided inputs into the data analysis and interpretation. Both authors reviewed the manuscript.

Funding Open Access funding enabled and organized by CAUL and its Member Institutions. The financial support through the School of Civil Engineering at the University of Queensland is acknowledged.

Declarations

Conflict of interest In line with recommendations of the Office of the Commonwealth Ombudsman (Australia), Hubert Chanson declares a conflict of interest with Matthias Kramer (UNSW, Canberra) and Stefan Felder (UNSW, Sydney).

References

1. Arosquipa Nina Y, Shi R, Wüthrich D, Chanson H (2022) Air–water flows and head losses on stepped spillways with inclined steps. J Irrig Drain Eng 148(11):15. https://doi.org/10.1061/(ASCE)IR.1943-4774.0001701
2. Arosquipa Nina Y, Shi R, Wüthrich D, Chanson H (2022) Intrusive and non-intrusive two-phase air-water measurements on stepped spillways: a physical study. Exp Therm Fluid Sci. https://doi.org/10.1016/j.expthermflusci.2021.110545
3. Bertrand J (1878) Sur l'homogénéité dans les formules de physique. Comptes rendus 86(15):916–920
4. Boes RM (2000) Zweiphasenströmung und Energieumsetzung an Grosskaskaden. ('Two-Phase Flow and Energy Dissipation on Cascades.') Ph.D. thesis, VAW-ETH, Zürich, Switzerland (in German)
5. Boes RM, Hager WH (2003) Hydraulic design of stepped spillways. J Hydraul Eng ASCE 129(9):671–679
6. Bradley JN, Peterka AJ (1957) The hydraulic design of stilling basins: short stilling basin for canal structures, small outlet works and small spillways (Basin III). J Hydr Div 83(HY5):1403–1411

7. Brocchini M, Peregrine DH (2001) The dynamics of strong turbulence at free surfaces. part 2. free-surface boundary conditions. J Fluid Mech 449:255–290
8. Bung DB (2009) Zur selbstbelüfteten Gerinnenströmung auf Kaskaden mit gemässigter Neigung. ('Self-aerated skimming flows on embankment stepped spillways.') Ph.D. thesis, University of Wuppertal, LuFG Wasserwirtschaft and Wasserbau, Germany, 292 pages (in German)
9. Bung DB, and Valero D (2015) Image processing for bubble image velocimetry in self-aerated flows. *Proc. 36th IAHR World Congress*, The Hague, The Netherlands, 27 June-3 July, 8 pages (CD ROM)
10. Cain P, Wood IR (1981) Measurements of self-aerated flow on a spillway. J Hydr Div 107(11):1425–1444
11. Cartellier A, Achard JL (1991) Local phase detection probes in fluid/fluid two-phase flows. Rev Sci Instrum 62(2):279–303
12. Castro AM, Li J, Carrica PM (2016) A mechanistic model of bubble entrainment in turbulent free surface flows. Int J Multiph Flow 86:35–55
13. Chamani MR (1997) Skimming Flow in a Large Model of a Stepped Spillway. *Ph.D. thesis*, Dept of Civil Eng., University of Alberta, Edmonton, Canada
14. Chamani MR, Rajaratnam N (1999) Onset of skimming flow on stepped spillways. J Hydr Eng 125(9):969–971
15. Chanson H (1993) Self-aerated flows on chutes and spillways. J Hydraul Eng ASCE 119(2):220–243. https://doi.org/10.1061/(ASCE)0733-9429(1993)119:2(220)
16. Chanson H (1995) Hydraulic design of stepped cascades, channels, weirs and spillways. Pergamon, UK, p 292
17. Chanson H (1995) Air bubble diffusion in supercritical open channel flow. proc. 12th australasian fluid mechanics conference AFMC, sydney, Australia, R.W. Bilger Editor 2:707–710
18. Chanson H (1997) Air bubble entrainment in free-surface turbulent shear flows. Academic Press, London, p 401
19. Chanson H (1999) The Hydraulics of Open Channel Flow: An Introduction. *Edward Arnold*, 1st edition, London, 512
20. Chanson H (2000) Historical development of stepped cascades for the dissipation of hydraulic energy. Transact Newcomen Soc 71(2):295–318. https://doi.org/10.1080/03720187.2000.12023617
21. Chanson H (2001) The hydraulics of stepped chutes and spillways. Balkema, Netherlands
22. Chanson H (2002) Air-water flow measurements with intrusive phase-detection probes. can we improve their interpretation? J Hydraul Eng 128(3):252–255. https://doi.org/10.1061/(ASCE)0733-9429(2002)128:3(252)
23. Chanson H (2009) Embankment overtopping protections system and earth dam spillways. in dams: impact, stability and design, nova science publishers, hauppauge NY, USA, Ed. W.P. Hayes and M.C. Barnes Chapter 4:101–132
24. Chanson H (2009) Turbulent air-water flows in hydraulic structures: dynamic similarity and scale effects. Environ Fluid Mech 9(2):125–142. https://doi.org/10.1007/s10652-008-9078-3
25. Chanson H (2013) Hydraulics of aerated flows: qui pro quo? J Hydraul Res IAHR, Invit Vis Paper 51(3):223–243. https://doi.org/10.1080/00221686.2013.795917
26. Chanson H (2015a) Energy dissipation in hydraulic structures. IAHR Monograph, CRC Press, Taylor & Francis Group, Leiden, Netherlands, p 168
27. Chanson H (2015b) Embankment overtopping protection systems. Acta Geotecnica 10(3):305–318. https://doi.org/10.1007/s11440-014-0362-8
28. Chanson H (2022) Stepped spillway prototype operation and air entrainment: toward a better understanding of the mechanisms leading to air entrainment in skimming flows. J Hydraul Eng 148(11):17. https://doi.org/10.1061/(ASCE)HY.1943-7900.0002015
29. Chanson H (2022) On air entrapment onset and surface velocity in high-speed turbulent prototype flows. Flow Measurement Instrum. https://doi.org/10.1016/j.flowmeasinst.2022.102122
30. Chanson H, Bung D, and Matos J (2015) Stepped spillways and cascades. In: Energy Dissipation in Hydraulic Structures. *IAHR Monograph*, CRC Press, Taylor & Francis Group, Leiden, The Netherlands, H. Chanson Editor, pp. 45–64
31. Chanson H, Toombes L (2002) Air-water flows down stepped chutes: turbulence and flow structure observations. Int J Multiph Flow 28(11):1737–1761. https://doi.org/10.1016/S0301-9322(02)00089-7
32. Chanson H, Whitmore RL (1998) Gold creek dam and its unusual waste waterway (1890–1997): design, operation, maintenance. Canadian J Civil Engin 25(4):755–768. https://doi.org/10.1139/cjce-25-4-755
33. Chanson H, Yasuda Y, Ohtsu I (2002) Flow resistance in skimming flows and its modelling. Can J Civ Eng 29(6):809–819. https://doi.org/10.1139/L02-083

34. Chanson H, Arosquipa Nina Y (2024) Momentum and energy considerations in self-aerated free-surface flows. Environ Fluid Mech. https://doi.org/10.1007/s10652-024-09978-w
35. Chaokitka N, and Chanson H (2022) Hydraulics of a broad-crested weir with rounded edges: physical modelling.IN: Proceedings of 30th Hydrology and Water Resources Symposium HWRS2022, Brisbane, Australia, 30 November-2 December, Published by Engineers Australia, Brisbane, Australia, Paper 07, pp. 43–52
36. Elder RA (1984) Scaling is Vital to the Practicing Engineer. In: Proceedings International Symposium on Scale Effects in Modelling Hydraulic Structures, IAHR, Esslingen, Germany, H. Kobus Editor, General Lecture, Paper 0.1, 3 p
37. Ervine DA, Falvey HT (1987) Behaviour of turbulent water jets in the atmosphere and in plunge pools. Proc Inst Civil Eng 83:295–314
38. Felder S (2013) Air-Water Flow Properties on Stepped Spillways for Embankment Dams: Aeration, Energy Dissipation and Turbulence on Uniform, Non-Uniform and Pooled Stepped Chutes. Ph.D. thesis, School of Civil Engineering, The University of Queensland, Australia
39. Felder S, Chanson H (2009) Turbulence, dynamic similarity and scale effects in high-velocity free-surface flows above a stepped chute. Exp Fluids 47(1):1–18. https://doi.org/10.1007/s00348-009-0628-3
40. Gonzalez CA (2005) An Experimental Study of Free-Surface Aeration on Embankment Stepped Chutes. *Ph.D. thesis*, Department of Civil Engineering, The University of Queensland, Brisbane, Australia
41. Gordienko PI (1978) Reinforced-concrete-earth overflow dams. Dams & Spillways 61(2):3–17
42. Halbronn G (1952) Etude de la mise en régime des ecoulements sur les ouvrages à forte pente. applications au problème de l'entraînement d'air. Jl La Houille Blanche 3:347–371
43. Halbronn G. Durand R, and Cohen de Lara G (1953). Air Entrainment in Steeply Sloping Flumes. *Proc. 5th IAHR Congress*, IAHR-ASCE, Minneapolis, USA, pp. 455–466
44. Hager WH, Schleiss AJ, Boes RM, Pfister M (2021) Hydraulic engineering of dams. CRC Press, The Netherlands
45. Henderson FM (1966) Open channel flow. MacMillan Company, New York
46. Hendrickson K, Weymouth GD, Yu X, Yue DKP (2019) Wake behind a three-dimensional dry transom stern. Part 1. flow structure and large-scale air entrainment. J Fluid Mech 875:854–883
47. Hino M (1961) On the Mechanism of Self-Aerated Flow on Steep Slope Channels. Applications of the Statistical Theory of Turbulence. *Proc. 9th IAHR Congress*, Dubrovnick, Yugoslavia, pp. 123–132
48. Hunt SL, Kadavy KC (2011) Inception point relationship for flat-slopped stepped spillways. J Hydraul Eng 137(2):262–266
49. Icold (2017) Technical Advancements in Spillway Design—Progress and Innovations from 1985 to 2015. Bulletin 172, International Commission on Large Dams (ICOLD)
50. Keller RJ (1972) Field Measurement of Self-Aerated High Speed Open Channel Flow. Ph.D. thesis, Dept. of Civil Eng., Univ. of Canterbury, New Zealand.
51. Killen JM (1968) The Surface Characteristics of Self-Aerated Flow in Steep Channels. Ph.D. thesis, University of Minnesota, Minneapolis, USA
52. Kobus H (1984). Scale Effects in Modelling Hydraulic Structures. Institut fur Wasserbau, Universitat Stuttgart, IAHR International Symposium on Scale Effects in Modelling Hydraulic Structures, IAHR, Esslingen, Germany
53. Kobus H (1991) Introduction to Air-Water Flows. In: Air Entrainment in Free-Surface Flows, IAHR Hydraulic Structures Design Manual No. 4, Hydraulic Design Considerations, Balkema Publ., Rotterdam, The Netherlands, I.R. WOOD Editor, pp. 1–28
54. Kolkman PA (1984) Considerations about the Accuracy of Discharge Relations of Hydraulic Structures and the Use of Scale Models for their Calibration. In: Proceedings International Symposium on Scale Effects in Modelling Hydraulic Structures, IAHR, Esslingen, Germany, H. Kobus Editor, p11
55. Kramer M, Valero D (2023) Linking turbulent waves and bubble diffusion in self-aerated open-channel flows: two-state air concentration. J Fluid Mech 966:17
56. Levi E (1965) Longitudinal streaking in liquid currents. J Hydraul Res 3(2):25–39
57. Lubin P, Glockner S (2015) Numerical simulations of three-dimensional plunging breaking waves: generation and evolution of aerated vortex filaments. J Fluid Mech 767:364–393. https://doi.org/10.1017/jfm.2015.62
58. Matos J (1999) Emulsionamento de ar e dissipação de energia do escoamento em descarregadores em degraus. (Air entrainment and energy dissipation in flow over stepped spillways.) *Ph.D. thesis*, IST, Lisbon, Portugal (in Portuguese)
59. Matos J (2000) Hydraulic Design of Stepped Spillways over RCC Dams. Intl Workshop on Hydraulics of Stepped Spillways, Zürich, Switzerland, H.E. Minor & W.H. Hager Editors, Balkema Publ., pp. 187–194

60. Michels V and Lovely M (1953) Some Prototype Observations of Air Entrained Flow. Proc. 5th IAHR Congress, IAHR-ASCE, Minneapolis, USA, pp. 403–414
61. Novak P, Moffat AIB, Nalluri C and Narayanan R (2007). Hydraulic Structures. Taylor & Francis, London, UK, 4th edition, p700
62. Phillips M. and Ridette K. (2007). Computational fluid dynamics models and physical hydraulic modelling—do we need both? The design of the Hinze Dam Stage 3. Proc. 2007 NZSOLD/ANCOLD Conference, 8 pages
63. Phillips M (2020) Hydraulic Structures—Learning from Recent (Partial) Failures and the Opportunities They Present. In: Proceedings of the 8th IAHR International Symposium on Hydraulic Structures ISHS2020, 12–15 May 2020, Santiago, Chile, R. Janssen and H. Chanson Editors, The University of Queensland, Brisbane, Australia, Keynote paper, 24 pages https://doi.org/10.14264/uql.2020.515.
64. Rajaratnam N (1990) Skimming flow in stepped spillways. J Hydraul Eng ASCE 116(4):587–591
65. Roache, P.J. (2009). "Perspective: Validation - What does it mean?" *Journal of Fluids Engineering*, ASME, Vol. 131, March, Paper 034503, 4 pages.
66. Rouse H (1938) Fluid mechanics for hydraulic engineers. McGraw-Hill Publ, New York
67. Serizawa A, Kataoka I, Michiyoshi I (1975) Turbulence structure of air-water bubbly flows—i. measuring techniques. Int J Multiph Flow 2(3):221–233
68. Shi R, Wüthrich D, Chanson H (2023) Air-water properties of unsteady breaking bore part 2: void fraction and bubble statistics. Int J Multiph Flow 159:14. https://doi.org/10.1016/j.ijmultiphaseflow.2022.104337
69. Sorensen RM (1985) Stepped spillway hydraulic model investigation. J Hydraul Eng ASCE 111(12):1461–1472
70. Straub LG, Anderson AG (1958) Experiments on self-aerated flow in open channels. J Hydraul Div 84(HY7):1–35
71. Straub LG, and Lamb OP (1953) Experimental Studies of Air Entrainment in Open-Channel Flows. *Proc. 5th IAHR Congress*, IAHR-ASCE, Minneapolis, USA, pp. 425–437
72. Tang R, Zhang J, Bai R, Wang H (2022) Transverse nonuniformity of air-water flow and lateral wall effects in quasi-two-dimensional hydraulic jump. J Irrigat Drain Eng 148(10):16. https://doi.org/10.1061/(ASCE)IR.1943-4774.0001697
73. Toombes L (2002) Experimental Study of Air-Water Flow Properties on Low-Gradient Stepped Cascades. *Ph.D. thesis*, Dept of Civil Engineering, The University of Queensland, Brisbane, Australia.
74. Toombes L, Chanson H (2007) Surface waves and roughness in self-aerated supercritical flow. Environ Fluid Mech 7(3):259–270. https://doi.org/10.1007/s10652-007-9022-y
75. Toombes L, Chanson H (2008) Interfacial aeration and bubble count rate distributions in a supercritical flow past a backward-facing step. Int J Multiph Flow 34(5):427–436. https://doi.org/10.1016/j.ijmultiphaseflow.2008.01.005
76. Toro JP, Bombardelli FA, Paik J, Meireles I, Amador A (2016) Characterization of turbulence statistics on the non-aerated skimming flow over stepped spillways: a numerical study. Environ Fluid Mech 16:1195–1221. https://doi.org/10.1007/s10652-016-9472-1
77. USBR (1965). Design of Small Dams. *Bureau of Reclamation*, US Department of the Interior, Denver CO, USA, 1st edition
78. Vaschy A (1892) Sur les lois de similitude en physique. Annal Télégraphiques 19:25–28 (**(in French)**)
79. Volkart P, and Rutschmann, P (1984) Rapid Flow in Spillway Chutes with and without Deflectors—A Model-Prototype Comparison. *Proc. Intl. Symp. on Scale Effects in Modelling Hydraulic Structures*, IAHR, Esslingen, Germany, H. KOBUS editor, paper 4.5
80. Wahl TL, Frizell KW, Falvey HT (2019) Uplift pressures below spillway chute slabs at unvented open offset joints. J Hydraul Eng 145(11):11. https://doi.org/10.1061/(ASCE)HY.1943-7900.0001637
81. Wahrheit-Lensing A (1996) Selbstbelüftung une Energieumwandlung beim Abfluss über Treppenförmige Entlastungsanlagen. (Self-Aeration and Energy Dissipation in Flow iver Stepped Spillways.) *Ph.D. thesis*, Institute for Hydromechanics, Karlsruhe University, Germany, 164 pages
82. Wood IR (1984) Air Entrainment in High Speed Flows. *Proc. International Symposium on Scale Effects in Modelling Hydraulic Structures*, IAHR, Esslingen, Germany, H. Kobus editor, paper 4.1, 7 pages
83. Wood IR (1985) Air Water Flows. *Proc. 21st IAHR Congress*, Melbourne, Australia, Keynote address, pp. 18–29
84. Wood IR (1991). Air Entrainment in Free-Surface Flows. *IAHR Hydraulic Structures Design Manual No. 4*, Hydraulic Design Considerations, Balkema Publ., Rotterdam, The Netherlands, 149 pages

85. Wood IR, Ackers P, Loveless J (1983) General method for critical point on spillways. J Hydraul Eng ASCE 109(2):308–312
86. Wüthrich D, Shi R, Chanson H (2023) Transverse nonuniformity of air-water flow and lateral wall effects in quasi-two-dimensional hydraulic jump. discussion. J Irrigat Drain Eng 149(4):5. https://doi.org/10.1061/JIDEDH.IRENG-10047
87. Wüthrich D, Shi R, Wang H, and Chanson H (2020). Three-dimensional air-water flow properties of a hydraulic jump with low Froude numbers and relatively high Reynolds numbers.In: *Proceedings of the 8th IAHR International Symposium on Hydraulic Structures ISHS2020*, 12–15 May 2020, Santiago, Chile, R. Janssen and H. Chanson Editors, The University of Queensland, Brisbane, Australia, 10 pages https://doi.org/10.14264/uql.2020.583
88. Yasuda Y, and Chanson H. (2003). Micro- and Macro-scopic Study of Two-Phase Flow on a Stepped Chute. *Proc. 30th IAHR Biennial Congress*, Thessaloniki, Greece, J. Ganoulis and P. Prinos Editors, Vol. D, pp. 695–702.
89. Zabaleta F, Bombardelli FA, Toro JP (2020) Towards an understanding of the mechanisms leading to air entrainment in the skimming flow over stepped spillways. Environ Fluid Mech 20:375–392. https://doi.org/10.1007/s10652-019-09729-2
90. Zabaleta F, and Bombardelli FA (2020). "Eddy-resolving Simulation of Flows over Macroroughness. In: Proceedings of RiverFlow2020, CRC Press, UIJTTEWAAL et al. Editors, pp. 1293–1299
91. Zhang G (2017). Free-Surface Aeration, Turbulence, and Energy Dissipation on Stepped Chutes with Triangular Steps, Chamfered Steps, and Partially Blocked Step Cavities. *Ph.D. thesis*, The University of Queensland, School of Civil Engineering, https://doi.org/10.14264/uql.2017.906
92. Zhang G, Chanson H (2016) Interactions between Free-surface aeration and total pressure on a stepped chute. Exp Thermal Fluid Sci 74:368–381. https://doi.org/10.1016/j.expthermflusci.2015.12.011
93. Zhang G, Chanson H (2017) Self-aeration in the rapidly- and gradually-varying flow regions of steep smooth and stepped spillways. Environ Fluid Mech 17(1):27–46. https://doi.org/10.1007/s10652-015-9442-z
94. Zhang G, Chanson H (2018) Application of local optical flow methods to high-velocity free-surface flows: validation and application to stepped chutes. Exp Thermal Fluid Sci 90:186–199. https://doi.org/10.1016/j.expthermflusci.2017.09.010
95. Zhou H (1996). Hydraulic Performances of Skimming Flow over Stepped Spillway. Proc. 10th APDIAHR Congress, Langkawi Island, Malaysia, pp. 1–8